coatings

Article

Tribological and Corrosion Performance of CrAlN/CrN Coatings in Artificial Seawater under Varied Nitrogen Pressures

Man Li [1,*], Yunjiang Yu [2], Changwei Zou [3], Canxin Tian [3] and Yanxiong Xiang [3]

[1] Faculty of Mechanical and Electrical Engineering, Lingnan Normal University, Zhanjiang 524048, China
[2] Faculty of Chemistry and Chemical Engineering, Lingnan Normal University, Zhanjiang 524048, China
[3] Faculty of Physics Science and Technology, Lingnan Normal University, Zhanjiang 524048, China
* Correspondence: oqlm@163.com

Abstract: This study employed arc ion plating technology to deposit CrAlN/CrN coatings on stainless steel substrates, adjusting deposition pressures ranging from 1.0 Pa to 4.0 Pa. A detailed analysis of the coatings' microstructure, wear, and corrosion features was performed using X-ray diffraction, scanning electron microscopy, nanoindentation, tribometers, profilometers, and electrochemical workstations. The study revealed that the crystalline structure of the CrAlN/CrN coatings primarily consists of cubic crystals of AlN, (Cr, Al)N, and CrN. Diffraction peak intensity analysis revealed preferential orientation in the CrAlN coatings along the (111) and (200) crystal planes. As the pressure increased to 3.0 Pa, the content of Al elements peaked, and the columnar structure became denser; at this point, the H/E* ratio reached a maximum of 0.079, indicating excellent delamination and fracture resistance of the CrAlN/CrN coating at this pressure. Tests in artificial seawater environments showed that with the increase in nitrogen pressure, the friction coefficient gradually decreased, reaching its lowest at 3 Pa, approximately 0.19. The wear rate trend aligned with the friction coefficient, recorded at a mere 2.20×10^{-7} mm^3/Nm. Electrochemical polarization curve tests revealed that at 3 Pa pressure, the CrAlN/CrN coating had a corrosion potential of −0.04 V, a polarization resistance of 9.28×10^5 $\Omega \cdot cm^2$, and a very low corrosion current of 4.81×10^{-8} A/cm^2, demonstrating excellent corrosion resistance.

Keywords: CrAlN/CrN coatings; corrosion resistance; wear mechanism; artificial seawater

Citation: Li, M.; Yu, Y.; Zou, C.; Tian, C.; Xiang, Y. Tribological and Corrosion Performance of CrAlN/CrN Coatings in Artificial Seawater under Varied Nitrogen Pressures. *Coatings* **2023**, *13*, 2090. https://doi.org/10.3390/coatings13122090

Academic Editors: Francisco J. Flores-Ruiz and Saideep Muskeri

Received: 20 November 2023
Revised: 8 December 2023
Accepted: 13 December 2023
Published: 15 December 2023

1. Introduction

Components such as gears, bearings, and propellers in marine engineering equipment face the dual challenges of wear and corrosion due to prolonged exposure to seawater [1–3]. Specifically, 316 stainless steel, widely used for its excellent corrosion resistance, shows limitations in corrosive salt-based seawater environments [4]. The synergy of corrosion and wear, particularly studied in simulated environments like artificial seawater, reveals complex interactions during the damage and recovery of the material's passive layer [5–7]. Creating protective coatings on material surfaces through various deposition processes is an effective way to enhance the wear and corrosion resistance of marine equipment materials. This not only significantly extends the service life of marine equipment but also ensures its safe operation, making it a key research topic in the field of marine engineering.

CrN coatings, known for their superior antioxidation, corrosion, and wear resistance on surfaces of marine engineering equipment, are ideal for safeguarding materials like 316 stainless steel [8,9]. Often prepared through physical vapor deposition (PVD) methods, these coatings notably improve the wear and corrosion resistance of materials in marine settings. However, the columnar crystalline structure of CrN coatings may allow the penetration of chloride ions from seawater into the coating's micro-gaps, potentially leading to corrosion of the underlying substrate material [10,11].

Coatings in corrosive mediums like seawater are prone to various defects, such as porosity, particles, or voids. These flaws can not only accelerate corrosion but also lead to

the formation of microcracks on the coating surface, eventually causing delamination or spalling. To address these challenges, researchers are dedicated to improving the microstructure and crystal arrangement of coatings to reduce porosity and enhance compactness [12]. Notably, the solubility of Al elements in the CrN lattice makes the microstructure of CrAlN coatings denser and significantly reduces porosity. These changes in crystal and microstructure greatly influence the coating's corrosion behavior. Ding et al. [13] used a transverse rotating cathode arc system to deposit CrAlN and TiAlN coatings about 3 μm thick. They found the best corrosion resistance in NaCl solutions with Cr/Al and Ti/Al atomic ratios around 1:1, attributed to increased compactness and roughness of the coating as aluminum content rose. Wang et al. [14] prepared CrAlN nanocomposite films with varying aluminum content using reactive magnetron sputtering. The results showed that compared to CrN films, CrAlN nanocomposite films have smaller grain sizes and denser structures, with a hardness of about 33.4 GPa, thus exhibiting superior wear resistance.

Based on these research findings, the innovative design of composite-structured CrAlN-based nano coatings not only marks a new direction in surface coating technology but also addresses specific challenges in enhancing the wear and corrosion resistance of such coatings. This design reduces residual stress in the coating and enhances the adhesion between the coating and the substrate, effectively inhibiting crack propagation. As a result, it not only improves the hardness and wear resistance of CrAlN-based coatings but also optimizes their corrosion resistance. Employing multi-arc ion plating technology, Guo and colleagues [15] applied CrN, CrAlN, and CrAlN/CrN coatings on Ti6Al4V substrates. They found that the composite coating interface effectively suppresses crack propagation, thereby improving the coating's resistance to corrosion. Furthermore, the CrAlN/CrN composite coating exhibited the best anti-erosion performance, attributed to its high hardness and fracture toughness.

Despite numerous achievements in the field of CrAlN/CrN coating research, exploration regarding the impact of different deposition pressures on CrAlN/CrN coating performance remains insufficient. Hence, this study aims to fill this research gap by finely tuning deposition pressures to optimize the performance of CrAlN/CrN coatings. In this research, we employed multi-arc ion plating technology to deposit CrAlN/CrN composite coatings on 316 stainless steel substrates. Through precise pressure control during the deposition process and the use of advanced characterization techniques, we comprehensively analyzed the coating's microstructure, wear, and corrosion resistance. This comprehensive study not only demonstrates the effectiveness of pressure regulation in optimizing coating performance but also provides new insights into the relationship between the microstructure of CrAlN/CrN coatings and their macroscopic properties.

2. Experimental Details

2.1. Coating Deposition

This study utilized CrAlN/CrN coatings produced through the AS510DTXB multi-arc ion plating system by Beijing Danpu Surface Technology Co., Ltd., Beijing, China. Substrates used included 316 stainless steel and single crystal silicon wafers, each 20 mm × 20 mm × 2 mm in size. Target materials of high purity, comprising 99.9 at.% atomic CrAl alloy (30:70 ratio) and pure Cr, were symmetrically mounted inside a 540 mm × 300 mm × 400 mm vacuum coating chamber. Every target, measuring 100 mm in diameter and 20 mm in thickness, was set at least 200 mm away from the center of the target to the center of the substrate, as illustrated in Figure 1. The deposition process maintained a controlled atmosphere and vacuum environment through a gas flow control system that injected Ar and N_2 gases, in addition to a pumping system. A schematic of the deposition system's structure is shown in Figure 1.

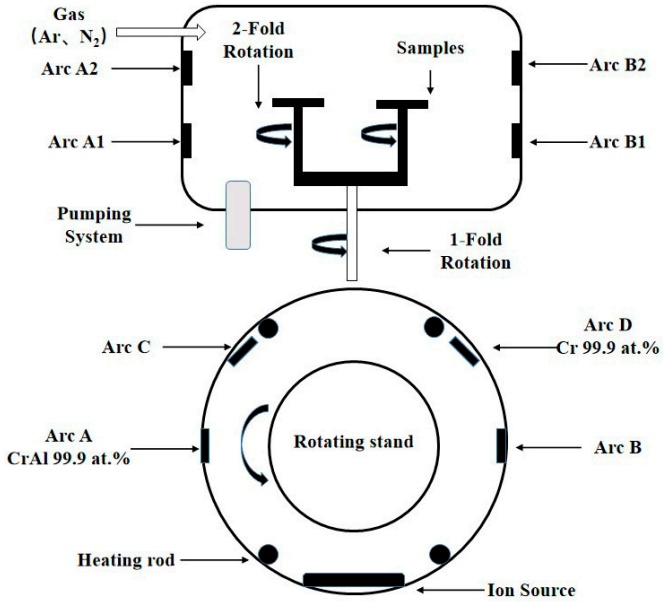

Figure 1. Schematic diagram of arc deposited CrAlN/CrN coatings.

Prior to preparation, the substrate materials were ultrasonically cleaned in acetone and anhydrous ethanol for 10 min each, air-dried with argon, and placed on the planetary target rack at the center of the vacuum chamber. The chamber was initially evacuated to 3.0×10^{-3} Pa using a high vacuum system consisting of a mechanical pump, Roots pump, and magnetically levitated turbo molecular pump, and then heated to 350 °C at 5 °C/min before starting the coating process. The coating deposition involved three key phases: initial Ar^+ ion cleaning by injecting 99.9 at.% pure argon to achieve a vacuum of 8.0×10^{-2} Pa, setting a pulse bias of −800 V with an 80% duty cycle for 30 min to remove surface oxides and impurities. Next, the Cr target's arc power was activated, with the current set to 80 A and nitrogen gas introduced. Operating in vacuum priority mode, the process maintained a stable working pressure of 3.0 Pa to deposit the CrN transition layer for a duration of 2 min. Lastly, the CrAl and Cr target arc power sources were activated with the current also set to 80 A and a bias of −100 V. Nitrogen gas was used and the working pressures were adjusted to 1.0 Pa, 2.0 Pa, 3.0 Pa, and 4.0 Pa over a 120 min deposition period. To maintain film layer uniformity, the planetary target rack was kept rotating at 3 r/min. See Table 1 for detailed deposition parameters.

Table 1. Deposition parameters of CrAlN/CrN coatings.

Pressure/Pa	CrAlN/CrN			
	Current/A	Pressure/Pa	Biasvoltage/V	Time/min
1.0, 2.0, 3.0, 4.0	80	3.0	−100 V	120

2.2. Characterization

The coatings' crystal structure was analyzed using an X-ray diffractometer (Bruker, Karlsruhe, Germany; Fällanden, Switzerland). The surface morphology, wear tracks, frictional wear patterns, and cross-sectional images were examined using a field emission scanning electron microscope (JEOL, Tokyo, Japan), and the chemical composition was determined using an EDS spectrometer (Thermo Fisher Inc., Waltham, MA, USA). The friction coefficient of the coating was determined using a tribometer (CMT-1, Huahui Instrument Company, Lanzhou, China), and the wear track morphology was analyzed using an optical profilometer (Bruker Contour GT K 3D, Billerica, Middlesex, MA, USA). Friction tests in artificial seawater utilized a 4 mm diameter Al_2O_3 ball, producing 8 mm

diameter wear tracks. The rotational speed was maintained at 5 m/min for a duration of 100 min. The wear rate of the coating's wear tracks was calculated using Equation (1) [16]:

$$ws, b = \frac{2\pi rA}{FL} \quad (1)$$

In the formula, F represents the test load, measured in Newtons (N); L stands for the friction length, in meters (m); r denotes the radius of the coating's wear scar, in millimeters (mm); and A signifies the average wear area of the coating's wear scar, in square millimeters (mm^2).

The coating's electrochemical behavior in artificial seawater was investigated using an electrochemical station (PGSTAT100N, AutoLab, Karlsruhe, Germany). The artificial seawater composition adhered to ASTM D1141-98 standards [17], with specifics listed in Table 2. Electrochemical Impedance Spectroscopy (EIS) was performed in open circuit potential (OCP) mode with a 10 mV sinusoidal wave disturbance across a frequency range of 0.01 Hz to 100,000 Hz. Potentiodynamic polarization curves were scanned from −1.0 to 1.0 V at a 20 mV/min scan rate. Corrosion current density (icorr) and corrosion potential (Ecorr) were determined by Tafel extrapolation and polarization resistance was calculated using the Stern–Geary equation [18]:

$$icorr = \frac{\beta_a \beta_c}{2.303 R_p (\beta_a + \beta_c)} \quad (2)$$

Table 2. Chemical composition of artificial seawater.

Component	NaCl	KCl	Na_2SO_4	$NaHCO_3$	$MgCl_2$	KBr	$CaCl_2$	H_3BO_3	$SrCl_2$	NaF
Concentration (g/L)	24.530	0.695	4.090	0.201	5.200	0.101	1.160	0.027	0.025	0.003

In Equation (2), β_a is the Tafel slope for anodic polarization, while β_c is the Tafel slope for cathodic polarization.

3. Results and Discussion

3.1. Morphology and Structure of the Coatings

Figure 2 illustrates the surface morphology of CrAlN/CrN coatings fabricated under varying nitrogen gas pressures, each showing typical arc ion plating defects such as particles, pinholes, and melt pits ranging in size from hundreds of nanometers to a few micrometers [19]. Figure 2a, showing the surface at a nitrogen pressure of 1.0 Pa, reveals a rough surface with numerous large particles. As pressure reaches 3.0 Pa, there is a marked reduction in the size and number of large particles, enhancing surface quality. This improvement stems from increased nitrogen flow at higher pressures, facilitating a more complete reaction between sputtered particles and nitrogen, thus reducing large particle formation. Additionally, higher nitrogen flow aids in forming high-melting-point nitrides on the surface, which reduces droplet evaporation and improves surface quality.

Figure 3 shows changes in Cr, Al, and N element concentrations in the coating at different nitrogen pressures. As the nitrogen pressure increases, there is an increase in N content within the coating; Al content first rises from 20.03 at.% to 23.22 at.%, then declines to 18.60 at.%; Cr content initially falls from 33.10 at.% to 26.56 at.%, then climbs to 30.21 at.%; the Al/Cr ratio first rises, then falls. These variations are primarily attributed to the increased collision probability of Cr and Al ions with nitrogen due to higher nitrogen pressures, significantly impacting the film deposition process through plasma physics kinetics and surface diffusion kinetics [20,21]. In particular, at a nitrogen pressure of 3.0 Pa, substituting larger Al atoms for Cr atoms in the lattice decreases the Cr proportion and increases the Al proportion, raising the Al/Cr ratio. Moreover, when the nitrogen pressure reaches 4.0 Pa, there is a relative increase in Cr content and a decrease in Al content within the coating, resulting in a decrease in the Al/Cr ratio. This phenomenon

can be explained from the perspectives of ion bombardment theory and plasma physics, particularly at higher nitrogen pressures, where Al ions, having a smaller mass-to-charge ratio, are more likely to deviate from the centrally located substrate under the influence of negative bias, causing a decrease in the proportion of Al in the coating while the proportion of Cr increases.

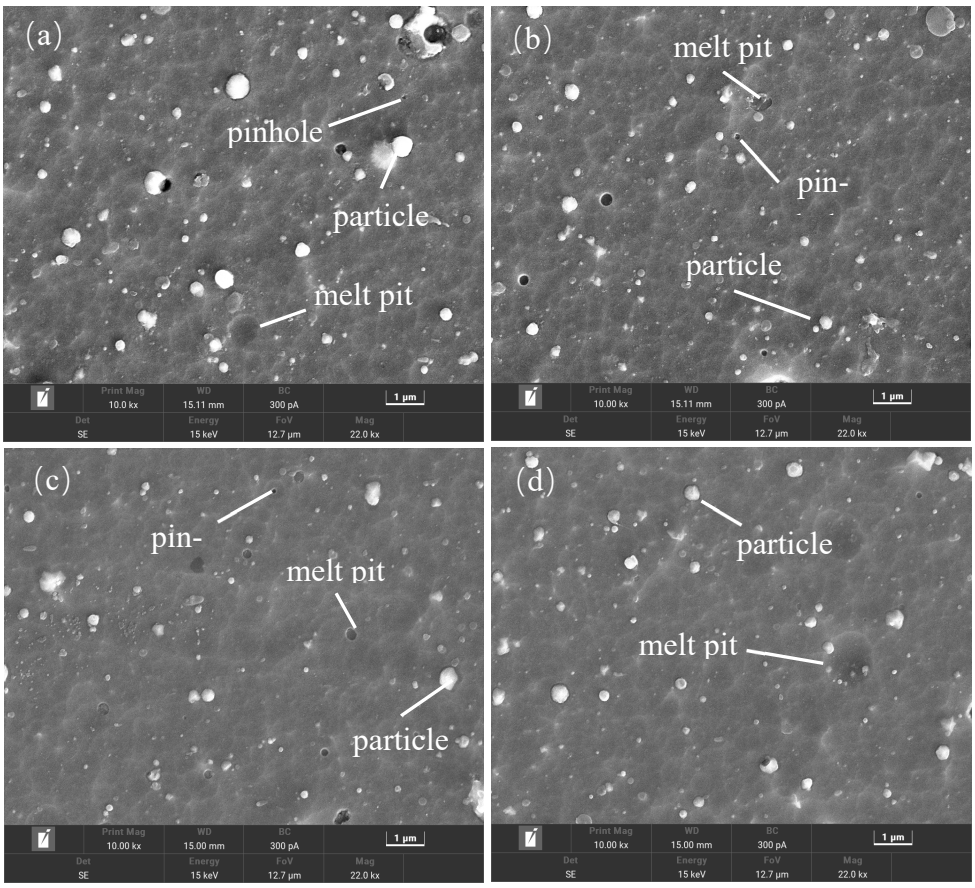

Figure 2. Surface Morphology of CrAlN/CrN Coatings under Different Nitrogen Pressures: (**a**) 1.0 Pa; (**b**) 2.0 Pa; (**c**) 3.0 Pa; (**d**) 4.0 Pa.

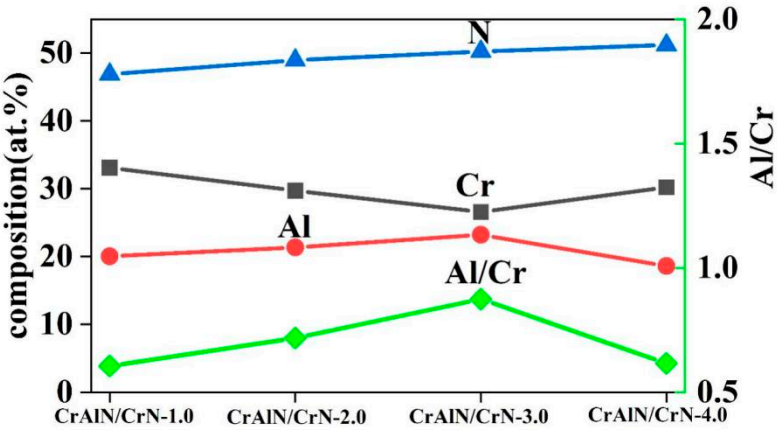

Figure 3. Elemental Composition and Al/Cr Ratio of CrAlN/CrN Coatings under Different Nitrogen Pressures.

Figure 4 presents cross-sectional SEM images of CrAlN/CrN coatings fabricated under varying nitrogen gas pressures, showing distinct structural changes correlating with increased nitrogen deposition pressure. At lower pressures of 1.0 Pa and 2.0 Pa, the coatings

exhibit a typical columnar crystalline structure, indicating growth dominated by grain competition and columnar growth mechanisms. As the nitrogen pressure increases to 3.0 Pa, the columnar structure becomes more refined and compact, attributed to increased Al content disrupting CrN crystal growth. However, at a further increased nitrogen pressure of 4.0 Pa, the deviation of Al ions from the substrate is more pronounced, reducing the proportion of Al in the coating and increasing that of Cr, which may lead to an adjustment in the crystal structure and growth mechanisms of the coating. Wuhrer et al. [22] demonstrated that increasing nitrogen pressure alters the chemical composition and phase structure of coatings, affecting their surface morphology and deposition rate. The phenomenon of 'target poisoning' at high nitrogen pressures, where excessive nitrogen reduces the deposition rate of the sputtering target, leads to thinner coatings. This explains why coatings deposited at 4.0 Pa are thinner than those at lower nitrogen pressures.

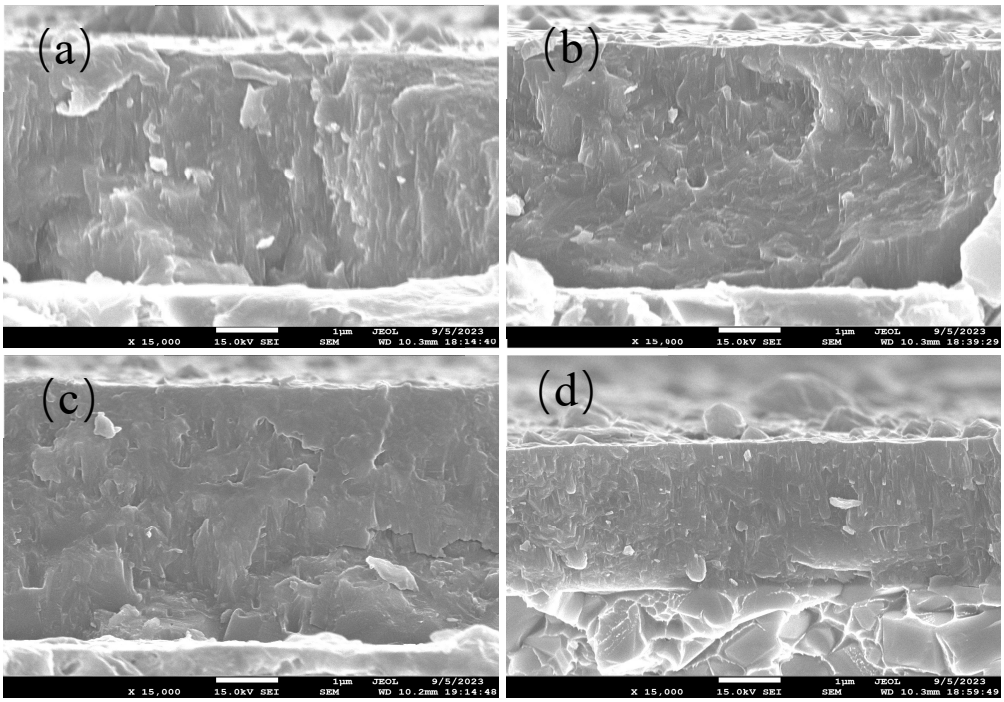

Figure 4. Cross-sectional Morphologies of CrAlN/CrN Coatings at Different Nitrogen Pressures: (**a**) 1.0 Pa; (**b**) 2.0 Pa; (**c**) 3.0 Pa; (**d**) 4.0 Pa.

Figure 5 and its enlarged inset showcase the X-ray diffraction (XRD) patterns of CrAlN/CrN coatings deposited under various nitrogen pressures, confirming a cubic phase structure akin to CrN. With changes in nitrogen pressure, the diffraction peak intensity of (Cr,Al)N (111) remains stable, whereas the intensity of (Cr,Al)N (200) increases, suggesting fine-tuning of the lattice components. Detailed observation of the (Cr,Al)N (111) peak in the magnified image shows that, although peak intensity changes slightly, the half-peak width broadens, typically associated with changes in grain size. Together with the increased intensity of the (Cr,Al)N (200) diffraction peak, these observations suggest that with increasing nitrogen pressure, the substitution of Al for Cr atoms in the lattice becomes more pronounced, leading to smaller lattice parameters and finer grains [23].

Figure 6 shows the changes in hardness (H), elastic modulus (E), and H/E* ratio of CrAlN/CrN coatings with nitrogen gas pressure. The coatings' microstructure and mechanical properties significantly depend on nitrogen pressure. Deposited at a nitrogen pressure of 1.0 Pa, the CrAlN/CrN-1.0 coating exhibits a hardness of 28.7 ± 1.0 GPa and an elastic modulus of 386.3 ± 8.8 GPa. With increasing deposition pressure, both hardness and elastic modulus rise, reaching peak values of 33.2 ± 1.1 GPa and 415.1 ± 17.5 GPa at 3 Pa, respectively. However, a further increase in pressure to 4.0 Pa leads to a decline

in both properties, with hardness and elastic modulus dropping to 28.4 ± 1.0 GPa and 388.2 ± 6.3 GPa, respectively. The H/E* ratio, a key indicator of mechanical performance, reflects the coating's resistance to elastic and plastic deformation and is related to wear resistance. With increasing deposition pressure, the H/E* ratio first increases to a peak and then decreases. The highest H/E* ratio of 0.079, observed at 3.0 Pa, suggests that the CrAlN/CrN-3.0 coating exhibits superior resistance to delamination and fracture. This improvement is likely due to high nitrogen pressure enhancing Al atom reactivity and concentration, leading to a finer, more compact columnar structure, which disrupts CrN crystal growth and increases hardness and wear resistance by impeding dislocation movement [24].

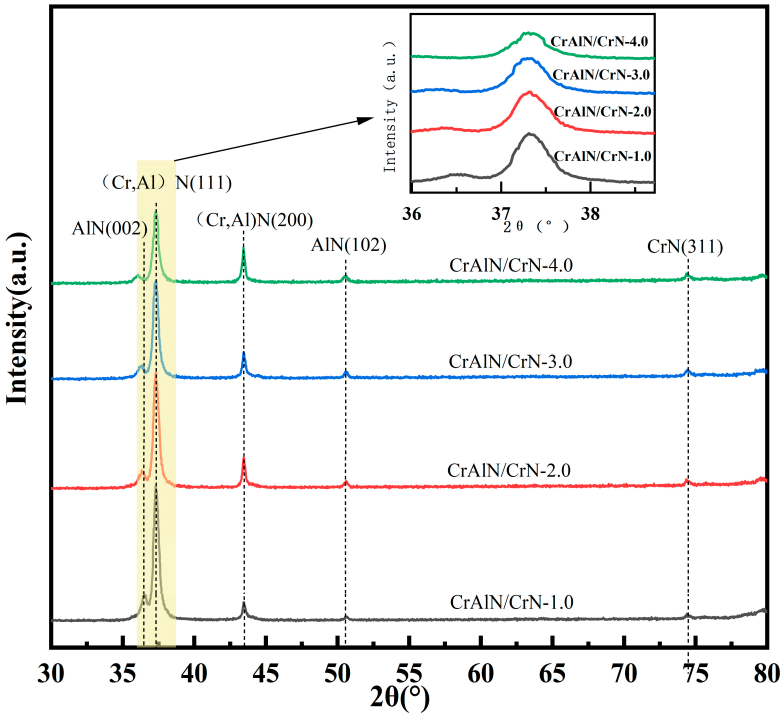

Figure 5. X-Ray Diffraction of CrAlN/CrN Coatings at Different Nitrogen Pressures.

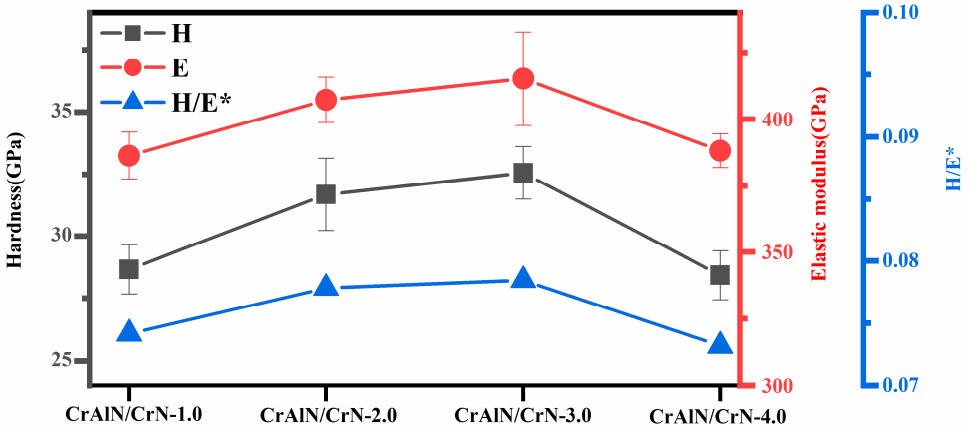

Figure 6. Indentation Hardness, Elastic Modulus, and H/E* Ratios of CrAlN/CrN Coatings under Different Nitrogen Pressures.

3.2. The Wear Performance of the Coatings in Artificial Seawater

Figure 7 displays the friction coefficient trends and average steady-state coefficients for CrAlN/CrN coatings at varying nitrogen pressures in synthetic seawater. Figure 7a shows the initial run-in phase with significant friction coefficient fluctuations due to larger surface

particles, indicating unstable friction. This phase is transient; as wear continues, these particles either integrate into the coating matrix or are eroded, leading to a smoother friction interface and a stabilized friction coefficient [25]. Specifically, the CrAlN/CrN-1.0 coating shows a friction coefficient reduction from 0.23 to 0.21 within the first 200 m of sliding, then fluctuates around 0.22. The CrAlN/CrN-2.0 coating displays a downward trend in friction coefficient within the first 175 m, stabilizing at around 0.22. The CrAlN/CrN-4.0 coating's friction coefficient fluctuates around 0.22 in the initial 230 m, then shows a steady increase, reaching a minimum of 0.24. Importantly, the CrAlN/CrN-3.0 coating exhibits outstanding tribological properties, with an initial increase in friction coefficient for the first 50 m, followed by a steady decrease to a minimum of 0.18. Figure 7b reveals that among the coatings, CrAlN/CrN-3.0 has the lowest average steady-state friction coefficient of 0.19, underscoring the synergy between deposition-induced microstructural refinement and enhanced wear resistance.

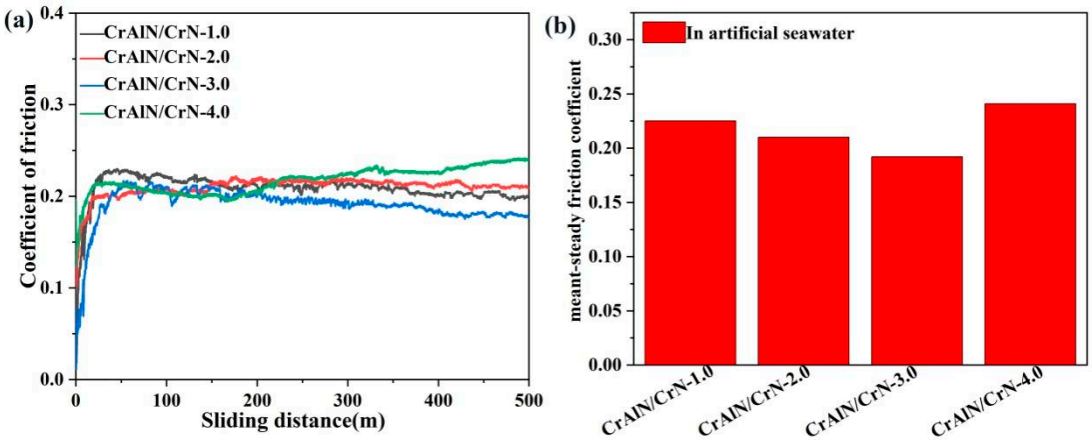

Figure 7. Friction Coefficient Curves (**a**) and Average Steady-State Friction Coefficients (**b**) of CrAlN/CrN Coatings at Different Nitrogen Pressures.

Figure 8 depicts the wear marks and EDS images of CrAlN/CrN coatings at different nitrogen pressures in artificial seawater. The SEM images reveal wear mark characteristics, indicating significant changes in the coating surface's wear properties with increasing deposition pressure. At the lower deposition pressures of 1.0 Pa and 2.0 Pa, wear marks show clear delamination layers and surface features, especially in the CrAlN/CrN-1.0 coating deposited at 1.0 Pa, exhibiting significant material removal or deformation. These features are likely related to high surface roughness and particle detachment, typically indicating lower hardness and modulus of elasticity of the coating. EDS analysis reveals the composition of elements like Cr, Al, N, O, Ca, and Mg in the coatings, particularly the presence of O, Mg, and Ca, which may indicate interactions of ions in the environment with the coating, including potential corrosion or material transfer phenomena. Such reactions could lead to decreased coating performance and increased wear likelihood. Coatings in this state are more susceptible to mechanical wear or corrosive effects. Specifically, in the CrAlN/CrN-1.0 coating deposited at 1.0 Pa, notable surface features and chemical element changes suggest significant corrosion and material removal under mechanical stress, likely linked to adhesive wear mechanisms where particle contact points in materials fracture and lead to material transfer during sliding [26]. Compared to lower pressures, coatings deposited at higher pressures (3.0 Pa and 4.0 Pa) show smoother wear tracks and reduced signs of corrosion in EDS spectra, suggesting a change in the wear mechanism of the coatings in artificial seawater. Coatings with higher H (hardness) and E (modulus of elasticity) values are superior in maintaining shape and resisting external forces, while a high H/E ratio indicates the coating's ability to maintain high hardness under pressure, reducing plastic deformation, effectively resisting wear, and maintaining stability [27]. For the CrAlN/CrN-3.0 coating deposited at 3.0 Pa, notable decreases in wear track depth and

enhanced edge smoothness indicate increased hardness and modulus of elasticity, as well as an improved H/E ratio, all indicative of the coating's stability under load.

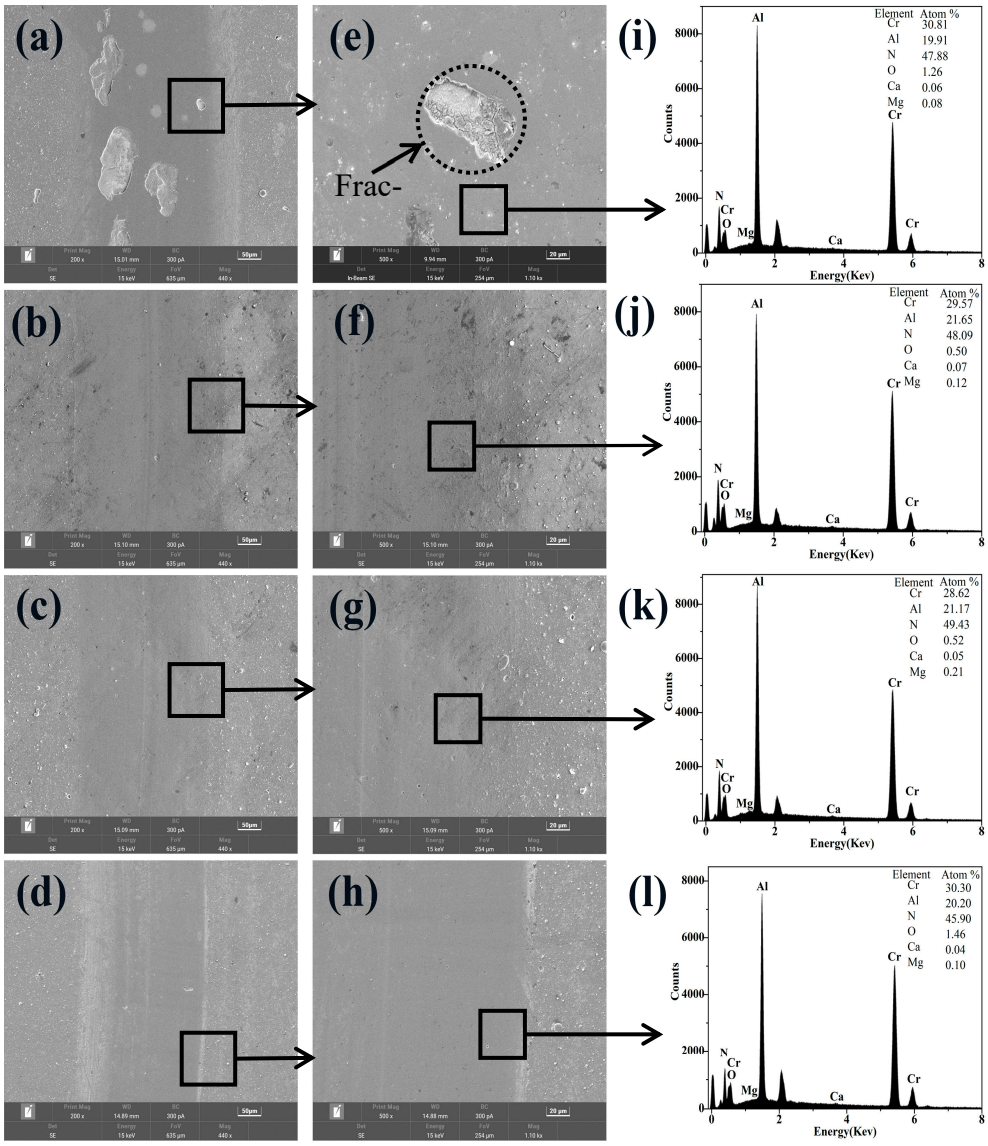

Figure 8. Wear track morphologies of CrAlN/CrN coatings under varying nitrogen pressures (**a**–**h**) and corresponding EDS spectra (**i**–**l**).

Figure 9 depicts the wear profile diagrams of CrAlN/CrN coatings at different nitrogen pressures in artificial seawater. In the CrAlN/CrN-1.0 coating, the largest width irregular transverse grooves are observed, characterized by two similarly sized grooves in the central area that gradually shallow towards the edges, suggesting an uneven response of the coating material to wear under specific pressure. Further observations reveal sharp longitudinal grooves with maximum depth in the CrAlN/CrN-2.0 coating, indicating a unique wear pattern under different deposition pressures. In contrast, the CrAlN/CrN-3.0 coating at higher pressures displays a significant reduction in wear track depth and increased smoothness of wear track edges, possibly reflecting better wear resistance and structural integrity of the coating formed under higher pressure. This emphasizes the key role of the microstructure formed at 3.0 Pa deposition pressure in enhancing the coating's wear resistance. However, at 4.0 Pa, the coating, despite exhibiting relatively shallow wear tracks, shows irregular small pits, hinting at potential alternative wear patterns. This observation may reflect that, although the coating maintains high hardness,

the microstructure formed under higher pressures could be more prone to surface fatigue and microcracking.

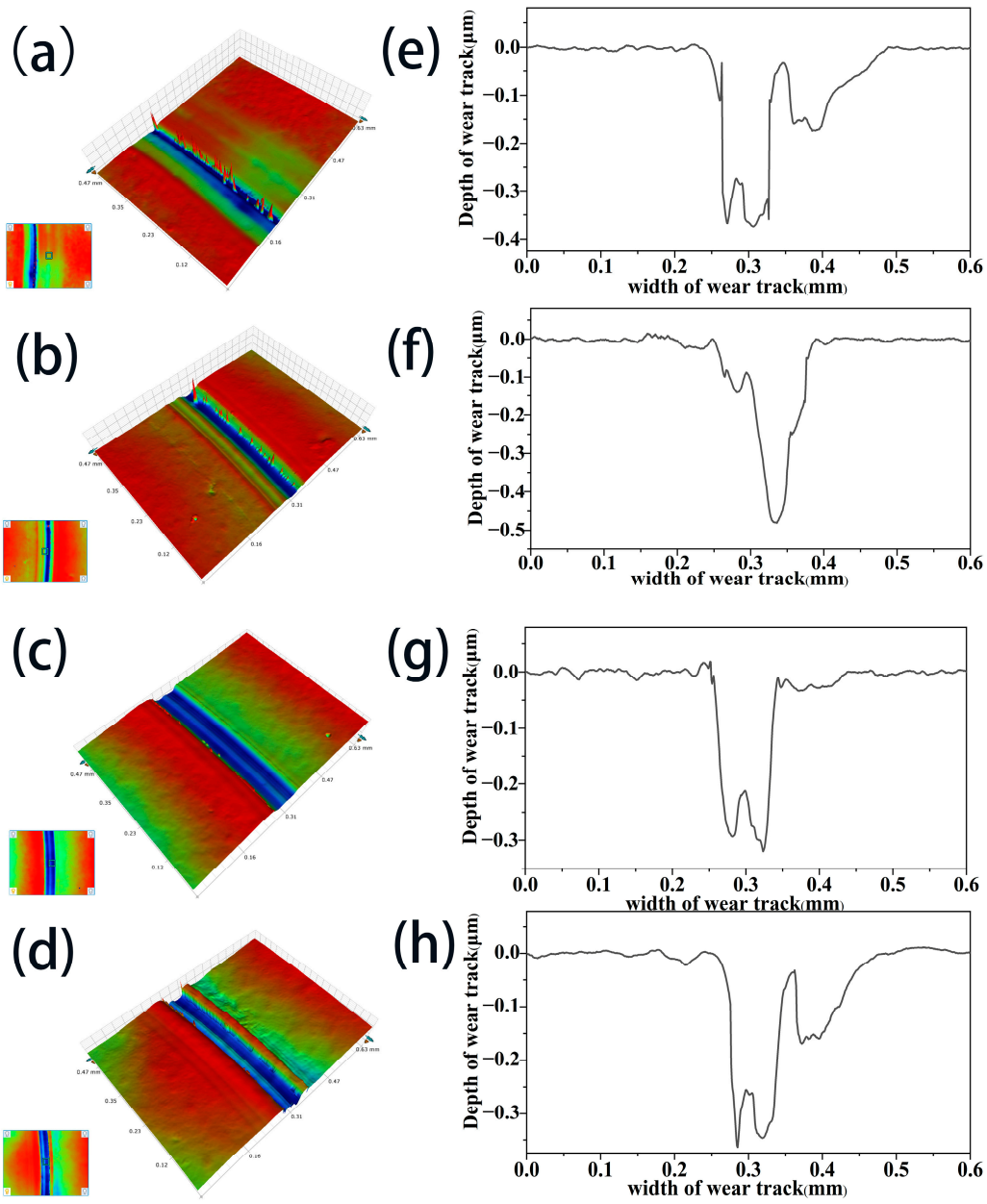

Figure 9. 3D contour maps (**a**–**d**) and wear track diagrams (**e**–**h**) of CrAlN/CrN coatings under different nitrogen pressures.

These findings indicate that the coating experiences distinct wear mechanisms under different deposition pressures. At lower pressures, abrasive and adhesive wear likely dominate, whereas, at higher pressures, wear may be predominantly influenced by surface fatigue. Particularly under 3.0 Pa conditions, the CrAlN/CrN-3.0 coating demonstrates excellent wear resistance, possibly related to its tighter microstructure and higher hardness and modulus of elasticity. These characteristics help the coating resist microstructural damage under repeated loading, thereby reducing wear.

Figure 10 illustrates the wear rates of CrAlN/CrN coatings at different nitrogen pressures in artificial seawater. Tribological assessments conducted in artificial seawater depict the relationship between the wear rates of CrAlN/CrN coatings and nitrogen pressure. After testing, the wear rate was highest at 1.0 Pa at 3.75 $\times$ 10^{-7} mm^3/Nm, lowest at 3.0 Pa

at 2.20 × 10^{-7} mm^3/Nm, and slightly increased to 3.18 × 10^{-7} mm^3/Nm at 4.0 Pa. With the coating's hardness (H), elasticity (E), and H/E ratio shown in Figure 6, CrAlN/CrN-3.0 coating at 3.0 Pa deposition pressure exhibited optimal tribological performance. The CrAlN/CrN-3.0 coating shows the highest hardness and modulus of elasticity, with an ideal H/E ratio, corresponding to its lowest recorded wear rate. This underscores the importance of a strengthened microstructure under optimal deposition parameters for wear resistance. Increased hardness usually correlates with better wear resistance, while a higher modulus of elasticity suggests the material's capacity to retain shape under load [28]. Additionally, an elevated H/E ratio is often seen as an indicator of wear resistance, as it denotes the material's capability to maintain hardness and resist plastic deformation under stress.

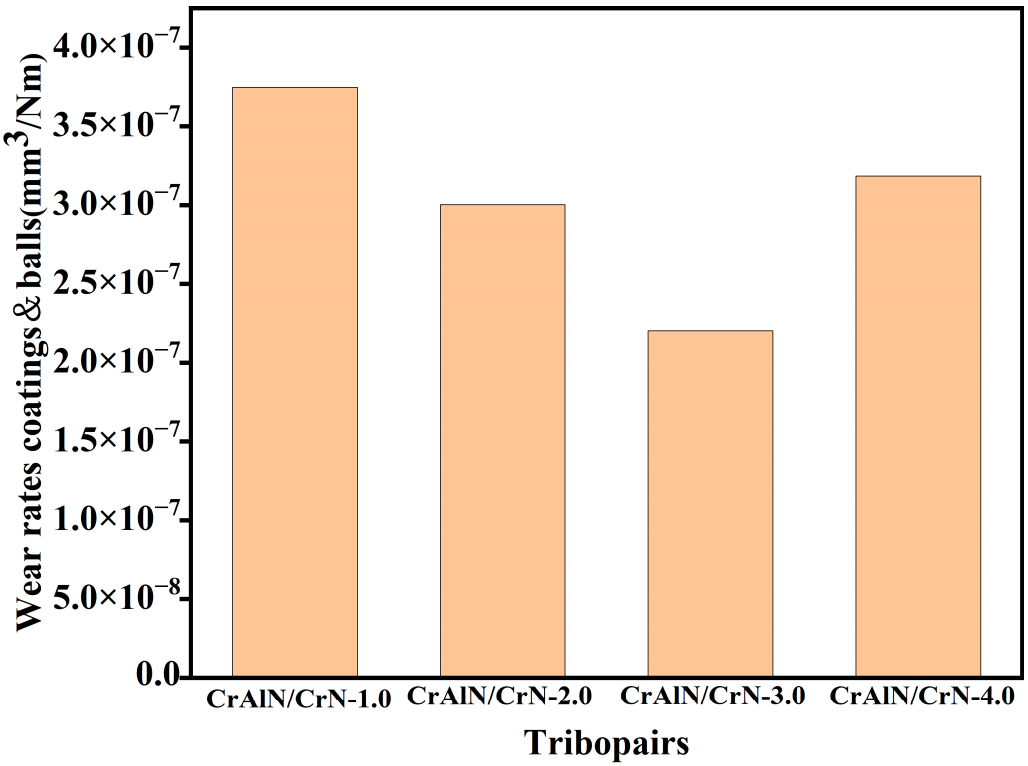

Figure 10. Wear Rates of CrAlN/CrN Coatings at Different Nitrogen Pressures.

Under a deposition condition of 4.0 Pa, the CrAlN/CrN-4.0 coating, despite a slight reduction in hardness, exhibited an increased wear rate compared to conditions at 2.0 Pa and 3.0 Pa. This suggests that higher nitrogen pressures might induce changes in the microstructure, potentially leading to weaker particle bonding or reduced grain boundary density, thereby affecting the overall wear resistance of the coating. In summary, deposition pressure markedly affects the microstructure and mechanical properties of CrAlN/CrN coatings. At a nitrogen pressure of 3.0 Pa, the coating shows the lowest wear rate, likely due to its finer grain structure and increased grain boundary density, which can enhance wear and corrosion resistance.

3.3. The Corrosion Performance of the Coatings in Artificial Seawater

Figure 11 demonstrates the correlations among the impedance modulus, phase angle, and frequency of the coating under different nitrogen pressures during Electrochemical Impedance Spectroscopy (EIS) tests, as well as the simulated circuit diagram. The EIS tests reveal that artificial seawater engages in electrochemical reactions with the coating's surface. Concurrently, the seawater seeps through micro-defects, like micropores, and undergoes electrochemical reactions at the substrate interface [29]. Figure 11a presents the Nyquist plots for the CrAlN/CrN coating during alternating current (AC) impedance tests,

showing capacitive-resistive arcs in all samples, including loops of varying diameters. In the high-frequency domain, the capacitive arcs are associated with the coating's resistance and capacitance, whereas, in the low-frequency domain, the capacitive reactance is related to the solution resistance and charge transfer resistance. Larger capacitive arcs indicate greater impedance, suggesting enhanced corrosion resistance of the coating [30,31]. The CrAlN/CrN-3.0 coating, with its prominent capacitive arc and elevated low-frequency impedance, showcases a robust barrier to corrosion agents. Figure 11b depicts the phase angle plots for the CrAlN/CrN coatings. Typically, a phase angle nearing 90 degrees indicates a more significant capacitive response of the coating, highlighting its efficiency in combating electrolytic corrosion. In the low-frequency range, impedance values are key indicators of the coating's corrosion resistance, with a higher low-frequency impedance modulus signifying superior resistance [32]. The elevated phase angle noted in the CrAlN/CrN-3.0 coating underscores its exceptional capacitive characteristics, crucial for assessing its corrosion protection efficacy. Considering frequency, the extensive frequency range accentuates the coating's remarkable capacitive capabilities, demonstrating its efficacy in shielding the substrate from seawater corrosion over a broader spectrum [33].

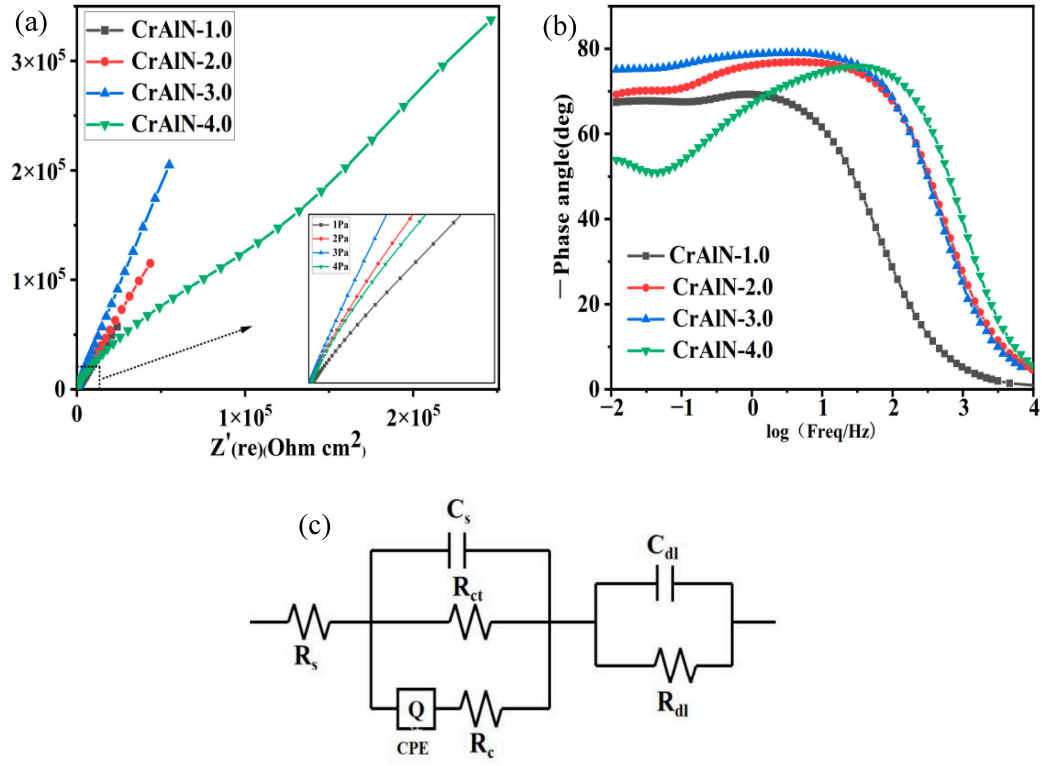

Figure 11. Nyquist Plots (**a**), Phase Angle Plots (**b**), and Equivalent Circuit Diagrams (**c**) of CrAlN/CrN Coatings at Different Nitrogen Pressures.

In the comparison of four coatings, the CrAlN/CrN-3.0 coating demonstrated the largest arc radius, the highest phase angle, and the broadest frequency range. This strongly suggests that the CrAlN/CrN-3.0 coating outperforms the others in terms of corrosion resistance.

ZSimpWin 3.6 software was utilized for fitting the experimental data, with the selection of a suitable equivalent circuit to delve deeper into the anticorrosion mechanism of the CrAlN/CrN coating system. The equivalent circuit representing the anticorrosion mechanism of the CrAlN/CrN coating system is depicted in Figure 11c. Table 3 lists the fitting parameters of the various coating systems.

Table 3. Fitted Results of Electrochemical Impedance Spectroscopy for CrAlN/CrN Coatings in Artificial Seawater at Different Nitrogen Pressures.

Sample	R_s ($\Omega \cdot cm^2$)	C_s ($F \cdot cm^{-2}$)	R_{ct} ($\Omega \cdot cm^2$)	CPE (Q)		R_c ($\Omega \cdot cm^2$)	C_s ($F \cdot cm^{-2}$)	R_{dl} ($\Omega \cdot cm^2$)
				Y_0 ($\Omega^{-1} \cdot sncm^{-2}$)	n			
CrAlN/CrN1	76.3	1.05×10^{-5}	2.94×10^{6}	1.10×10^{-4}	0.756	1.02	1.27×10^{-3}	5.57×10^{2}
CrAlN/CrN2	14.1	1.22×10^{-5}	2.28×10^{6}	5.65×10^{-5}	0.792	3.35	4.59×10^{-4}	2.69×10^{3}
CrAlN/CrN3	16.6	1.01×10^{-5}	1.85×10^{7}	3.37×10^{-5}	0.819	3.10	8.06×10^{-4}	2.44×10^{3}
CrAlN/CrN4	74	2.27×10^{-5}	2.17×10^{5}	8.46×10^{-6}	0.662	1.29×10^{3}	4.37×10^{-5}	1.22×10^{6}

Rs represents the solution resistance, while Cs indicates the capacitance between the working electrode and the electrolyte. Q (Constant Phase Element, CPE) can be considered a special capacitor reflecting the poor surface roughness of arc ion-plated coatings, signifying the coating's outer layer resistance, including R_c (coating resistance) [34]. Rct, the charge transfer resistance, is a key parameter characterizing the coating's resistive properties, with its value representing electron transfer along the surface. The double-layer capacitance (C_{dl}) and resistance (R_{dl}) represent the inner layer resistance of the coating [35]. As shown in Table 3, CrAlN/CrN coatings prepared under various pressures exhibit higher resistance values, with CrAlN/CrN-3.0 coating achieving an R_{ct} of 1.85×10^7, indicating the best corrosion performance.

Figure 12 illustrates the dynamic potential polarization curves of the coating in artificial seawater, along with the electrochemical values derived from these curves, as detailed in Table 4. E_{corr} and i_{corr} represent the corrosion potential and corrosion current density, respectively. E_{corr} characterizes the material's corrosion tendency from a thermodynamic perspective, while i_{corr} represents the instantaneous rate of corrosion reaction from a kinetic perspective. As the nitrogen gas pressure increases, the E_{corr} of the CrAlN/CrN coating shifts to a more positive area, gradually enhancing its corrosion inhibition performance. At a pressure of 1.0 Pa, the coating exhibits the lowest corrosion value of −0.11 V, indicating the weakest corrosion resistance. This is attributed to the prominent columnar structure of the coating at this pressure, which facilitates seawater penetration. With the increase in pressure, the i_{corr} value shows a decreasing trend, with the CrAlN/CrN-3.0 coating reaching the lowest value of 4.81×10^{-8}. This is an order of magnitude lower than other coatings, suggesting a slower corrosion rate for CrAlN/CrN-3.0, offering superior substrate protection. Conversely, further pressure increases produce contrary outcomes. In electrochemical research, especially in studies of corrosion and coatings, polarization resistance is a key parameter obtained from fitting electrochemical polarization curves. It offers a detailed understanding of the corrosion behavior of the materials or coatings under study [36]. The CrAlN/CrN-3.0 coating has the highest Rp value at 9.28×10^5 $\Omega \cdot cm^2$, further validating its exceptional corrosion resistance.

The combination of electrochemical impedance spectroscopy and polarization curve results has provided comprehensive insights into the corrosion resistance of CrAlN/CrN coatings at varying nitrogen gas pressures. Notably, the CrAlN/CrN-3.0 coating demonstrated superior corrosion resistance at a 3.0 Pa nitrogen gas pressure, a fact well-substantiated by electrochemical tests. The EIS results accentuated the largest capacitive arc and highest low-frequency impedance modulus of the CrAlN/CrN-3.0 coating, reflecting its considerable electrochemical stability and exceptional corrosion resistance at 3.0 Pa. These properties are intimately linked to the microstructural attributes of the coating, especially its refined grain structure and dense grain boundaries, effectively reducing corrosion media penetration and enhancing corrosion resistance. Polarization curve analysis further corroborates these findings. The positive shift in Ecorr, a notable reduction in i_{corr}, and a substantial increase in polarization resistance (Rp) reveal that the CrAlN/CrN-3.0 coating deposited under 3.0 Pa has a reduced corrosion propensity and a slower corrosion rate. These parameters, in conjunction with the EIS results, distinctly highlight the coating's superior performance in corrosion inhibition. In contrast, coatings under 1 Pa and 2.0 Pa conditions, due to their loose columnar crystal structure and larger grain boundary areas, are more susceptible to

corrosion media penetration, resulting in relatively weaker corrosion resistance. However, when the nitrogen gas pressure is increased to 4.0 Pa, there is a decline in the corrosion resistance of the coating, possibly related to changes in the microstructure, leading to a more pronounced columnar crystal structure. Overall, the optimized microstructure of the CrAlN/CrN-3.0 coating under 3.0 Pa nitrogen gas pressure is crucial for its enhanced corrosion resistance. This emphasizes the significance of microstructural optimization in improving the overall corrosion resistance of coatings.

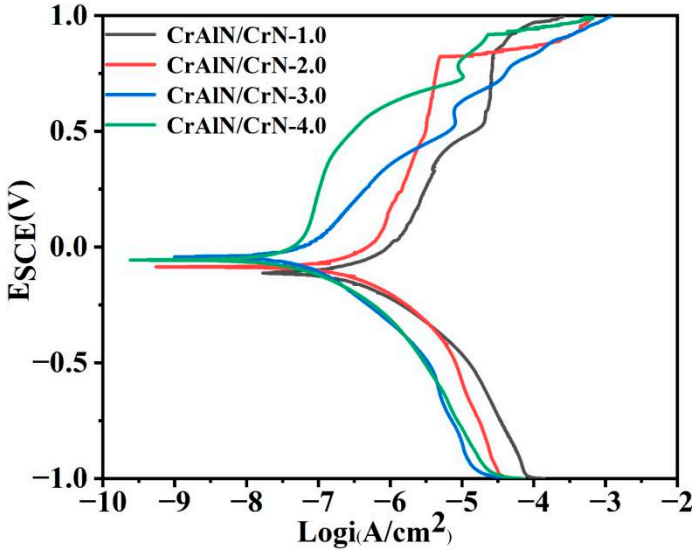

Figure 12. Tafel Curves of CrAlN/CrN Coatings in Artificial Seawater at Different Nitrogen Pressures.

Table 4. Electrochemical Corrosion Parameters Inferred from Tafel Plots.

Coatings	E_{corr} (V)	β_a (V)	β_c (V)	i_{corr} (A/cm^2)	R_p (Ω·cm^2)
CrAlN/CrN-1.0	−0.11	5.32	5.73	2.92×10^{-7}	1.35×10^{5}
CrAlN/CrN-2.0	−0.09	4.76	6.26	2.40×10^{-7}	1.64×10^{5}
CrAlN/CrN-3.0	−0.04	2.52	7.22	4.81×10^{-8}	9.28×10^{5}
CrAlN/CrN-4.0	−0.06	4.00	5.30	6.64×10^{-8}	7.04×10^{5}

4. Conclusions

This study successfully fabricated CrAlN/CrN coatings on 316 stainless steel substrates using multi-arc ion plating technology at different nitrogen gas pressures, thoroughly evaluating their microstructure, mechanical properties, wear performance, and corrosion resistance. The coatings primarily consisted of cubic crystals of AlN, (Cr, Al)N, and CrN, with the CrAlN coating showing significant preferential orientation on the (111) and (200) crystal planes. At a nitrogen pressure of 3.0 Pa, the coatings exhibited peak Al content, leading to a denser columnar structure and an increased H/E* ratio of 0.079, indicative of superior layering and crack resistance. This was confirmed in artificial seawater tests where the coating's friction coefficient decreased with rising nitrogen pressure, hitting a low of about 0.19 at 3.0 Pa. The corresponding wear rate was minimal at 2.20×10^{-7} mm^3/Nm. Electrochemical tests demonstrated that the CrAlN/CrN-3.0 coating at 3.0 Pa possessed exceptional corrosion resistance with a corrosion potential of −0.04 V, a polarization resistance of 9.28×10^5 Ω·cm^2, and a remarkably low corrosion current of 4.81×10^{-8} A/cm^2. This research highlights the critical importance of precise deposition pressure control in enhancing the properties of CrAlN/CrN coatings. At an optimal pressure of 3.0 Pa, the coating not only exhibited superior hardness and elasticity but also the most favorable H/E* ratio and a remarkably low rate of wear, demonstrating outstanding corrosion and wear resistance in artificial seawater environments. These findings provide valuable insights for the design and optimization of marine engineering equipment.

Author Contributions: Conceptualization, methodology, writing—review and editing, M.L.; visualization, data curation, Y.Y.; resources, supervision, C.Z.; visualization, investigation, C.T.; validation, Y.X. All authors have read and agreed to the published version of the manuscript.

Funding: This work was supported by the Innovation team project of Guangdong Universities (2020KCXTD032), Science and Technology Project of Zhanjiang (2019A03009, 2022A0100, 2023A21510, 2023B01012), Natural Science Foundation of Guangdong Province (2022A1515011137), and Lingnan Normal University Research Project (QN2117, LY2203).

Institutional Review Board Statement: Not applicable.

Informed Consent Statement: Not applicable.

Data Availability Statement: Data are contained within the article.

Conflicts of Interest: The authors declare no conflict of interest.

References

1. Wood, R.J.K. Marine wear and tribocorrosion. *Wear* **2017**, *376*, 893–910. [CrossRef]
2. Li, Z.; Yu, H.; Sun, D. The tribocorrosion mechanism of aluminum alloy 7075-T6 in the deep ocean. *Corros. Sci.* **2021**, *183*, 109306. [CrossRef]
3. Li, L.; Liu, L.L.; Li, X.; Guo, P.; Ke, P.; Wang, A. Enhanced tribocorrosion performance of Cr/GLC multilayered films for marine protective application. *ACS Appl. Mater. Interfaces* **2018**, *10*, 13187–13198. [CrossRef] [PubMed]
4. Kumaran, S.T.; Baranidharan, K.; Uthayakumar, M.; Padmanabhan, P. Corrosion Studies on Stainless Steel 316 and their Prevention-A Review. *INCAS Bull.* **2021**, *13*, 245–251. [CrossRef]
5. Albrimi, Y.A.; Eddib, A.; Douch, J.; Berghoute, Y.; Hamdani, M.; Souto, R.M. Electrochemical behaviour of AISI 316 austenitic stainless steel in acidic media containing chloride ions. *Int. J. Electrochem. Sci.* **2011**, *6*, 4614–4627. [CrossRef]
6. Kumar, N.; Kumar, A.; Singh, A.K.; Das, G. Corrosion resistance of austenitic Cr-Ni stainless steel in 1 M HCl. *Int. J. Mech. Eng. Robot. Res.* **2014**, *3*, 21.
7. Wu, D.; Guan, Z.; Cheng, Q.; Guo, W.; Tang, M.; Liu, Y. Development of a friction test apparatus for simulating the ultra-high pressure environment of the deep ocean. *Wear* **2020**, *452*, 203294. [CrossRef]
8. Aldrich-Smith, G.; Teer, D.G.; Dearnley, P.A. Corrosion-wear response of sputtered CrN and S-phase coated austenitic stainless steel. *Surf. Coat. Technol.* **1999**, *116*, 1161–1165. [CrossRef]
9. Shan, L.; Wang, Y.; Zhang, Y.; Zhang, Q.; Xue, Q. Tribocorrosion behaviors of PVD CrN coated stainless steel in seawater. *Wear* **2016**, *362*, 97–104. [CrossRef]
10. Vite, M.; Moreno-Ríos, M.; Hernández, E.G.; Laguna-Camacho, J. A study of the abrasive resistance of sputtered CrN coatings deposited on AISI 316 and AISI H13 steel substrates using steel particles. *Wear* **2011**, *271*, 1273–1279. [CrossRef]
11. Li, H.; Zhang, C.; Liu, C.; Huang, M. Improvement in corrosion resistance of CrN coatings. *Surf. Coat. Technol.* **2019**, *365*, 158–163. [CrossRef]
12. Wang, D.; Lin, S.; Yang, Z.; Yin, Z.-F.; Ye, F.-X.; Gao, X.-Y.; Qiao, Y.-P.; Xue, Y.-N.; Yang, H.-Z.; Zhou, K.-S. Failure mechanisms of CrN and CrAlN coatings for solid particle erosion resistance. *Vacuum* **2022**, *204*, 111313. [CrossRef]
13. Ding, X.; Tan, A.L.K.; Zeng, X.T.; Wang, C.; Yue, T.; Sun, C.Q. Corrosion resistance of CrAlN and TiAlN coatings deposited by lateral rotating cathode arc. *Thin Solid Film.* **2008**, *516*, 5716–5720. [CrossRef]
14. Wang, L.; Zhang, G.; Wood, R.J.K.; Wang, S.C.; Xue, Q. Fabrication of CrAlN nanocomposite films with high hardness and excellent anti-wear performance for gear application. *Surf. Coat. Technol.* **2010**, *204*, 3517–3524. [CrossRef]
15. Guo, H.; Sun, Q.; Zhou, D.; Yu, M.; Wang, Y.; Wang, Q.; Li, X. Erosion behavior of CrN, CrAlN and CrAlN/CrN multilayer coatings deposited on Ti6Al4V. *Surf. Coat. Technol.* **2022**, *437*, 128284. [CrossRef]
16. Wang, Q.; Zhou, F.; Wang, X.; Chen, K.; Wang, M.; Qian, T.; Li, Y. Comparison of tribological properties of CrN, TiCN and TiAlN coatings sliding against SiC balls in water. *Appl. Surf. Sci.* **2011**, *257*, 7813–7820. [CrossRef]
17. *ASTM G102-89e1*; Standard Practice for Calculation of Corrosion Rates and Related Information from Electrochemi cal Measurements. ASTM: West Conshohocken, PA, USA, 2015.
18. Wang, Q.; Zhou, F.; Zhou, Z.; Li, L.K.-Y.; Yan, J. An investigation on the crack resistance of CrN, CrBN and CrTiBN coatings via nanoindentation. *Vacuum* **2017**, *145*, 186–193. [CrossRef]
19. Goto, H.; Akao, N.; Hara, N.; Sugimoto, K. Pinhole Defect Density of CrNx Thin Films Formed by Ion-Beam-Enhanced Depo-sition on Stainless Steel Substrates. *J. Electrochem. Soc.* **2007**, *154*, C189. [CrossRef]
20. Bujak, J.; Walkowicz, J.; Kusiński, J. Influence of the nitrogen pressure on the structure and properties of (Ti, Al) N coatings deposited by cathodic vacuum arc PVD process. *Surf. Coat. Technol.* **2004**, *180*, 150–157. [CrossRef]
21. Paksunchai, C.; Chantharangsi, C. *CrAlN Film Hardness Uniformity Affected by Nitrogen Content*; AIP Publishing: Melville, NY, USA, 2020; Volume 2279.
22. Bin Abdullah, M.Z.; Bin Abdullah, A.N.; Bin Othman, M.H.; Ahmad, M.A.B.; Hussain, P. Mechanical properties of Cr/CrN/CrCN/ZrN multilayer coatings by physical vapour deposition (PVD). *Adv. Mater. Res.* **2016**, *1133*, 99–102. [CrossRef]

23. Wuhrer, R.; Yeung, W.Y. A comparative study of magnetron co-sputtered nanocrystalline titanium aluminium and chromium aluminium nitride coatings. *Scr. Mater.* **2004**, *50*, 1461–1466. [CrossRef]
24. Schlögl, M.; Kirchlechner, C.; Paulitsch, J.; Keckes, J.; Mayrhofer, P.H. Effects of structure and interfaces on fracture toughness of CrN/AlN multilayer coatings. *Scr. Mater.* **2013**, *68*, 917–920. [CrossRef]
25. Ye, Y.; Wang, Y.; Wang, C.; Li, J.; Yao, Y. An analysis on tribological performance of CrCN coatings with different carbon con-tents in seawater. *Tribol. Int.* **2015**, *91*, 131–139. [CrossRef]
26. Sui, X.; Liu, J.; Zhang, S.; Yang, J.; Hao, J. Microstructure, mechanical and tribological characterization of CrN/DLC/Cr-DLC multilayer coating with improved adhesive wear resistance. *Appl. Surf. Sci.* **2018**, *439*, 24–32. [CrossRef]
27. Beake, B.D. The influence of the H/E ratio on wear resistance of coating systems–Insights from small-scale testing. *Surf. Coat. Technol.* **2022**, *442*, 128272. [CrossRef]
28. Leyland, A.; Matthews, A. On the significance of the H/E ratio in wear control: A nanocomposite coating approach to optimised tribological behaviour. *Wear* **2000**, *246*, 1–11. [CrossRef]
29. Lu, C.Y.; Diyatmika, W.; Lou, B.S.; Lee, J.W. Superimposition of high power impulse and middle frequency magnetron sputtering for fabrication of CrTiBN multicomponent hard coatings. *Surf. Coat. Technol.* **2018**, *350*, 962–970. [CrossRef]
30. Ze, S.; Dejun, K.; Wei, L. Surface-interface microstructures and binding strength of cathodic arc ion plated TiCN coatings on YT14 cutting tools. *Surf. Interface Anal.* **2017**, *49*, 488–494. [CrossRef]
31. Ren, Y.; Babaie, E.; Bhaduri, S.B. Nanostructured amorphous magnesium phosphate/poly (lactic acid) composite coating for enhanced corrosion resistance and bioactivity of biodegradable AZ31 magnesium alloy. *Prog. Org. Coat.* **2018**, *118*, 1–8. [CrossRef]
32. Aissani, L.; Fellah, M.; Nouveau, C.; Abdul Samad, M.; Montagne, A.; Iost, A. Structural and mechanical properties of Cr–Zr–N coatings with different Zr content. *Surf. Eng.* **2020**, *36*, 69–77. [CrossRef]
33. Fu, Y.; Zhou, F.; Wang, Q.; Zhang, M.; Zhou, Z. Electrochemical and tribocorrosion performances of CrMoSiCN coating on Ti-6Al-4V titanium alloy in artificial seawater. *Corros. Sci.* **2020**, *165*, 108385. [CrossRef]
34. Zhu, G.; Cui, X.; Zhang, Y.; Chen, S.; Dong, M.; Liu, H.; Shao, Q.; Ding, T.; Wu, S.; Guo, Z. Poly (vinyl butyral)/graphene oxide/poly (methylhydrosiloxane) nanocomposite coating for improved aluminum alloy anticorrosion. *Polymer* **2019**, *172*, 415–422. [CrossRef]
35. Liu, S.; Gu, L.; Zhao, H.; Chen, J.; Yu, H. Corrosion resistance of graphene-reinforced waterborne epoxy coatings. *J. Mater. Sci. Technol.* **2016**, *32*, 425–431. [CrossRef]
36. Bard, A.J.; Faulkner, L.R.; White, H.S. *Electrochemical Methods: Fundamentals and Applications*; John Wiley& Sons: Hoboken, NJ, USA, 2022.